THE JOURNAL OF PHYSICAL CHEMISTRY B
A JOURNAL OF THE AMERICAN CHEMICAL SOCIETY

pubs.acs.org/JPCB

Article

Influence of CTAB Reverse Micellar Confinement on the Tetrahedral Structure of Liquid Water

Anupama Sharma, Mywish Anand, and Sudip Chakraborty*

Cite This: https://doi.org/10.1021/acs.jpcb.4c04773

Read Online

ACCESS | Metrics & More | Article Recommendations | Supporting Information

ABSTRACT: The effect of confinement on the tetrahedral ordering of liquid water plays a vital role in controlling their microscopic structure and dynamics as well as their spectroscopic properties. In this article, we have performed the classical molecular dynamics simulations of four different CTAB/water/chloroform reverse micelles with varied water content to study how the tetrahedral ordering of nanoscale water inside reverse micellar confinement influences the microscopic dynamics and the structural relaxation of water···water hydrogen bonds and its impact on the low-frequency intermolecular vibrational bands. We have noticed from the results obtained from simulated trajectories the lowering trends of tetrahedral ordering of water pools in reverse micellar confinements as we move from bulk to confined and strictly confined environments. We have observed that the order of confinements significantly altered the relaxation pattern of water···water hydrogen bonds present in the nanoscale water pool of reverse micelles. The recrossing related to hydrogen bond dynamics can effectively explain the relaxation pattern of $C_{HB}^{WW}(t)$ under confinement. The Br^{-1}··· water hydrogen bond depicts a much slower relaxation compared to the water···water hydrogen bonds inside reverse micelles. We have also explored the correlation between the tetrahedral ordering of nanoscale water pools and the relaxation of water···water hydrogen bonds with the 50 cm^{-1} band for water inside reverse micelles. The computations reported that compared to bulk water, the band appearing at 50 cm^{-1} for O···O···O triplet bending is nonuniformly blue-shifted by 18−45 cm^{-1} for the nanoscale water pool inside reverse micelles, and the intensity of the band drops from bulk to confined and strictly confined environments, which indicates the reduced tendency of such triplet formation. It is observed that a significant intensity variation at the 200 cm^{-1} band correlates with the effect of confinement on the tetrahedral ordering of the water pool inside reverse micelles. So, our observations support the influence of strictly confined environments on the tetrahedral water structure to adopt the quasi-two-dimensional water network and experience restricted longitudinal translations. It is further noticed that the 500 cm^{-1} librational band is also found to be blue-shifted by 71−112 cm^{-1} for the water pool in reverse micelles, and the extent of the shift being more noticeable for strictly confined environments correlates excellently with the sluggish relaxation of water···water hydrogen bonds in such environments.

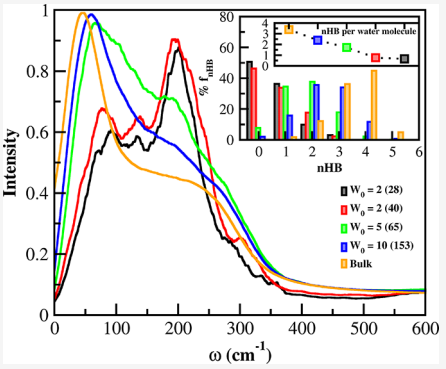

INTRODUCTION

Water, an essential chemical compound on earth, plays a diverse role in many complex environments.[1−5] With the potentiality of forming a hydrogen bond network in the bulk state, water also shows a distorted network in confined environments.[1,4,6−10] Water in a liquid state can be categorized as a tetrahedral liquid.[11] The water tetrahedral structure in confined environments may be distorted and show new phases[12−14] not normally seen in the same thermodynamic conditions, which can cause the anomalous behavior of water as compared to the normal bulk state.[15−17]

Specifically, reverse micellar systems could serve as an effective model for investigating confined aqueous pools due to their biological significance and industrial relevance.[18−21] These systems involve the study of water confined within reverse micelles (RMs), including cationic, anionic, zwitterionic, or nonionic surfactants.[22−24] The formation of reverse micellar systems is initiated by the amphiphilic nature of the surfactant molecules in nonpolar solutions with a small amount of polar solvents, typically water. The polar part of the surfactant forms the central core, creating a confined water pool, in order to minimize the unfavorable interactions between oil and water, thereby reducing interfacial tension.[25−27] The water pool confined inside RMs has been extensively studied due to its utility in drug delivery, nanomaterial synthesis, and its ability to solubilize enzymes and facilitate chemical catalysis.[28] The properties of the nanoscale water pool, along with its variations based on the water-to-surfactant molar ratio (W_0 = [H_2O/[surfactant]), are

Received: July 16, 2024
Revised: December 17, 2024
Accepted: December 18, 2024

an important factor in controlling the solvation and reactivity occurring at the core.

CTAB (cetyltrimethylammonium bromide) is a linear 16-hydrocarbon chain cationic surfactant with a headgroup consisting of quaternary ammonium covalently bonded with three methyl groups ($(C_{16}H_{33})N(CH_3)_3^+$ or CTA^+), and bromide anion (Br^-) was considered as a counterion in this study. The CTAB RMs consist of a hydrophilic core of water (H_2O) and an apolar chloroform ($CHCl_3$) solvent, constituting an L2 phase in a ternary system. In this configuration, the headgroup of the amphiphilic CTAB is oriented toward the water, with the hydrocarbon chains extending outward from it. This structural arrangement highlights the amphiphilic nature of CTAB, forming a distinct phase where the hydrophilic and hydrophobic components segregate into a well-defined core−solvent structure. CTAB RMs could be used as a model for the lipid to mimic cell membranes and determine the microenvironment of biomolecules such as proteins within the cellular environment.[29,30] CTAB RMs have also been employed as a medium for quantum dot synthesis, nanoparticle templating, and encapsulation of biomolecules.[31,32] It has been established as a dependable emulsifier for petroleum engineering applications.[33] It is well recognized for having properties of dispersion, suspension, solubilization, and transportation.[34−38] These properties make CTAB a unique compound to be mixed or interacted with other solutions or materials to form the emulsion.[33] Again, the size of the CTAB reverse micellar aqueous pool as well as the nature of interactions plays a crucial role in solubilization and extraction of an iron-binding protein lactoferrin.[39] Importantly, CTAB surfactant could provide sufficient hydrophilicity to facilitate the phase transfer of gold nanoparticles and render them water-soluble.[40] Hence, studying the properties of the aqueous phase inside CTAB RMs and their variation with RM size are interesting for both fundamental[41] and practical reasons considering that small pools of water can act as small microreactors or microbeakers.[42,43]

A substantial body of research is dedicated to the study of the structure and dynamics of nanoscale water pools present inside the RMs.[44−47] Importantly, the pump−probe techniques are suitable for probing the ultrafast dynamics of water in cationic,[48] anionic,[49−51] and phospholipid[52] RMs. To investigate the nature of water molecules through these experiments, the vibrations of the OH bond stretch are monitored via its excitation. Further, the core−shell model of nanoconfined water deciphers the nature of vibrational energy relaxation of interfacial water as well as the water present in the micellar core. Importantly, the spectral absorptions of the two kinds of water were found to be different. Bhattacharyya and co-workers have used fluorescence resonance energy transfer (FRET) to distinguish the behavior of water confined inside an AOT (bis(2-ethylhexyl) sulfosuccinate) RM.[53] In the report, they observed a very fast FRET from coumarin 480 (C480) to fluorescein 548 (F548) in the water pool of the AOT RM, which was absent in the case of bulk water. In another report, the OH-stretching mode lifetime of 800 fs was observed for water nanodroplets confined inside AOT RMs, indicating a strongly perturbed hydrogen-bond network and slower water dynamics.[54] Further, a reduction in OH-stretching lifetimes was also identified for RMs on augmentation of their sizes.[52,54] In addition, advanced infrared spectroscopy techniques have been at the forefront in studying the dynamical characteristics of water at various time scales.[55−57] In the recent past, Piletic et al. have studied the nanoscopic water pools of AOT RMs (1.7−4 nm diameter) with vibrational echo experiments and showed that the longer time scale dynamics of water are much slower than those observed for bulk water, while the fastest dynamics are very much similar to that of bulk water.[58] The observation illustrated that the slow dynamics of a nanoscale water pool confined inside RMs is a result of the confinement, in place of its ionic strength and nature. These charge-free confinement features of water are additionally supported by water trapped in other organic solvents (acetone)[59] and inside AOT lamellas.[60] The presence of different time scales suggests the exchange between the bulk and the interface of AOT/isooctane RMs.[51] In a separate observation, Angulo et al. have reported the two regimes of nanoscale water pool nature inside RMs. They monitored the reduced fluidity of confined water inside RMs as compared to the bulk water, which relates to the perturbed hydrogen bond network dynamics responsible for the altered proton-transfer process.[61]

Molecular dynamics (MD) simulation studies can provide insightful details of the structure and dynamics of water confined inside RMs and the structural aspects of RMs. The nature of water near the reverse micellar cavity interface is altered with the micellar size. In the recent past, Ladanyi and co-workers have simulated a spherical cavity of AOT surfactants in a nonpolar dielectric continuum, in which they observed highly restricted water near the cavity interface, due to the presence of large ion concentration there.[44] Kličová et al. have adopted a combined NMR and MD simulation-based approach to investigate the stability of aqueous pool confined inside CTAB RMs at subzero temperatures.[62] In their report, they observed the freezing of an aqueous pool below 233 K that becomes unstable upon cooling to relatively high temperatures (253 K). Rosenfeld and Schmuttenmaer reported a large slowdown in the dynamics at the interface and changes in water structure through the hydrogen bond network in the layers of water nearest to the AOT RM interface.[63] Ladanyi and co-workers have also presented several reports using a simplified model of water and AOT RMs to distinguish the confined aqueous pool into trapped, bound, and bulklike regions.[44,64,65] In earlier reports, the proposed core−shell model[66] for water confined inside Na-AOT RMs does not satisfy the results obtained by Pieniazek et al., where they rather suggest concavity of the interface is crucial.[67] As the concavity of the interface increases, it becomes increasingly difficult to find low-energy bifurcated hydrogen bond transition states necessary for rotational motion that ultimately reduces the reorientation.[67] Further, the weaker water-interface interaction inside cetyltrimethylammonium 1,4-bis(2-ethylhexyl) sulfosuccinate (CTA-AOT) RMs was reported by Falcone,[68] and with a water loading of W_0 = 20, a CTAB/hexanol mixture showed slow rotational diffusion compared with bulk throughout the water core, with the greatest slowing near the CTAB headgroups.[69] The interaction of confined water with the surfactant headgroup and the presence of a counterion alter the dynamics of water next to the cavity interface of RMs.[70] Interfacial water confined inside AOT RMs forms hydrogen bonds with the anionic sulfonate headgroups, whereas CTAB is shielded from intermolecular hydrogen bonding due to intervening methyl groups as reported in the previous studies.[71−73] Interestingly, the damped hydrogen bond dynamics within the pool of the RM system or at interfaces formed by the micelles have been reported extensively.[74−76] The computer simulation studies of other

https://doi.org/10.1021/acs.jpcb.4c04773
J. Phys. Chem. B XXXX, XXX, XXX−XXX

RMs have also depicted the damped motion of water in the solvation region of RMs.[77] In a recent study, we have observed the structural aspects of RMs as well as the differential behavior of nanoscale water pools confined inside RMs.[41]

The hydrogen bond dynamics belong to the unique characteristics of water, which assist the adaptation of anomalies in their behavior. Fluctuations and reorganizations of hydrogen bonds on time scales within 10 fs and 10 ps, connecting a disordered network of water molecules, give rise to these dynamics.[78] Monitoring the evolution of these hydrogen bond network dynamics holds tremendous importance in understanding the microscopic aspects of water. Hydrogen bond dynamics inside the confinement is another important issue. The regular hydrogen-bond network in bulk water gets disrupted inside confinement.[1,4,8,10,15] In the recent past, Ladanyi and co-workers have reported the multimolecular organization of water molecules in the hydrogen bond network inside the RMs by computing the number of hydrogen bonds at different radial locations.[65,79] Importantly, 2D IR spectroscopy can estimate hydrogen bond dynamics in subpicosecond time resolution.[80] Baiz and co-workers have used ultrafast 2D IR spectroscopy in conjunction with MD simulations to investigate the subps level solvation dynamics inside RMs with varied surfactant compositions.[81] They have observed differential behavior of the surfactant interfacial water dynamics and a significant slowdown of interfacial hydrogen bond dynamics in a heterogeneous surfactant mixture as compared to the homogeneous compositions. Alteration of the water hydrogen bond network due to the effect of confinement influences the low-frequency intermolecular vibrational spectrum of water in the terahertz and far-IR regions.[8,10,82,83] This suggests modifications of the water tetrahedral hydrogen-bonded network under confinement. Such modifications can be monitored by 2D IR, Raman spectroscopy, and THz spectroscopy techniques. Using IR spectroscopy, Sechler et al. have shown that the OH band absorptions altered as the micelle radius grew.[84] They characterized the OH absorption for interfacial and bulk water, corresponding to the weaker hydrogen bonding water network in the interfacial region as compared with the core/bulk. The near-infrared (NIR) spectral behavior of the water pool inside RMs is highly influenced by the surfactant polar groups and spatial confinement.[85] Recently, we have reported the structure and dynamics of confined water inside CTAB/water/chloroform RMs.[41] In this report, we have shown that the translational and reorientational dynamics of water pools in RMs are controlled by the nature of confinement. As a result, the present work aims to understand the microscopic dynamics and spectroscopic properties of water confined inside CTAB RMs with varied water loadings.

In order to investigate the influence of confinement on the microscopic dynamics and spectroscopy of nanoscale water inside CTAB/water/chloroform RMs, we have conducted classical MD simulations of four different CTAB/water/chloroform RMs with varied water loadings (Table 1). In this work, we explored the modification of the tetrahedral water network of nanoscale water pools under confinement and its influence on microscopic water dynamics and low-frequency vibrational bands. In this regard, we have computed various correlation functions including the ones that give information about the water triplet angle distribution along with the number of different kinds of hydrogen bond count. The dynamics of hydrogen bonds formed between water (water−water) and ion−water (Br^{-1}−water) molecules have been computed to investigate the microscopic dynamics of the nanoscale water pool and its dynamical transition in the presence of Br^{-1} ions inside four different RM systems, followed up with the velocity autocorrelation function and power spectral density of nanoscale water. This article is organized as follows: starting with the details of construction and setup of the reverse micellar systems, simulation methods are engaged in the present study, including the force fields. The detailed investigation of microscopic water dynamics and spectroscopic properties, as observed during the simulation in the form of different structural and correlation function analyses with their interpretation, has been reported in the Results and Discussion section. In the Conclusions section, we summarize the important findings from the study.

Table 1. Details of MD Simulations of CTAB/H_2O/$CHCl_3$ Reverse Micellar Systems[a]

system	W_0	N_s	R_w (Å)	σ_a (Å^2)	N_w	N_{CHCl3}
S1	2	28	7.5	45	56	6184
S2	2	40	8.4	45	80	6496
S3	5	65	13.4	45	324	7894
S4	10	153	22.4	45	1530	9271

[a]N_s stands for the surfactant aggregation number, R_w is the radius of the water pool, σ_a is the surface area per CTAB molecule, N_{CHCL3} is the number of chloroform molecules, and N_w is the number of water molecules present in the water pool for different values of W_0.

METHODOLOGY

System Setup and Simulation Details. We have constructed four different reverse micellar systems with water-to-surfactant ratios (W_0 = [H_2O]/[CTAB]) of 2, 2, 5, and 10, which were prepared using PACKMOL[86] and inserted into individual cubic boxes filled with chloroform.[87] In this work, the CTAB ($C_{19}H_{42}BrN$) RM with a water (H_2O) pool and apolar chloroform ($CHCl_3$) represents an L_2 phase ternary system where the polar headgroup of CTAB is placed toward water and the hydrocarbon tail toward chloroform. The simulation setups based on the experimental report by Klan and co-workers[62] and Lang et al.,[88] along with their compositions, are listed in Table 1. Initially, RM simulations starting from a predetermined spherical geometry are a common practice to reduce the computational time. Vasquez and co-workers demonstrated that starting from a predetermined spherical geometry or a random configuration has no effect on the resultant structure and properties of the RM.[89] For bulk water, a cubic box of 2500 water molecules was prepared as well for pure water properties. Topology and the GROMOS96 53a6-consistent[90] CTAB parameters were taken from a recent report,[91] along with the $CHCl_3$[92,93] interaction parameters. The SPC/E potential[94] was opted to model the water molecules, completely consistent with the chosen surfactant force field. Recently, Maiti and co-workers have reported that the SPC/E water model is the optimum choice for the structure, dynamics, and thermodynamics properties of water under graphitic confinement.[10,95] The simulation experiment on the constructed reverse micellar systems was commenced by eliminating the unfavorable contacts via steepest descent energy minimization, followed up with an equilibration at constant temperature (T = 298.15 K) and volume (NVT). The NVT equilibration was carried out for 3 ns duration, and an NPT simulation run was continued for 1

https://doi.org/10.1021/acs.jpcb.4c04773
J. Phys. Chem. B XXXX, XXX, XXX−XXX

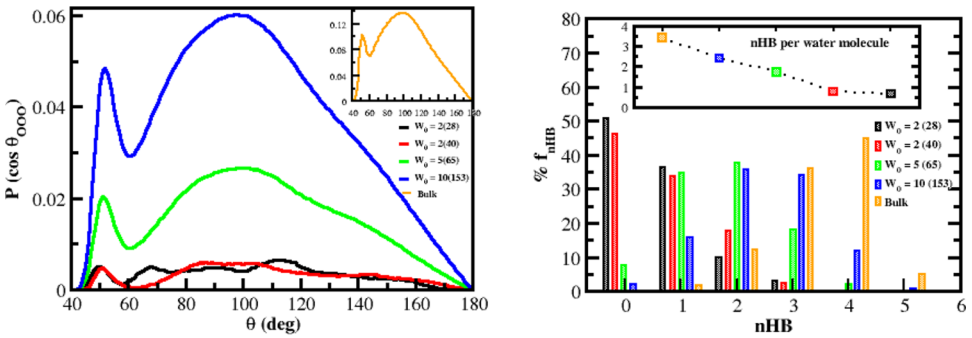

(a) (b)

Figure 1. (a) O−O−O triplet angle distribution functions $P(\cos\theta_{OOO})$ of water inside four different RMs (Table 1). (b) Population of hydrogen-bonded states and the average number of hydrogen bonds per water molecule (inset of Figure 1) for four different RMs. The results for bulk water are incorporated for comparison. Color code: black for W_0 = 2 RM with n_{CTAB} = 28; red for W_0 = 2 RM with n_{CTAB} = 40; green for W_0 = 5 RM with n_{CTAB} = 65; blue for W_0 = 10 RM with n_{CTAB} = 153; and orange for the bulk SPC/E water.

ns. Further, the equilibration of the system was extended via a production simulation run of 300 ns in the *NPT* ensemble, at constant temperature (T = 298.15 K) and pressure (P = 1.0 atm), with simulated trajectories stored at every 100 ps interval. An *NVT* simulation run with 1 ps resolution was further continued for 10 ns duration to estimate the dynamic properties of water inside the RM. Further, a 5 fs high-resolution trajectory of 50 ps time was also stored to probe the spectroscopic properties of nanoscale water.

We carried out classical MD simulations corresponding to the four reverse micellar systems with varied water-to-surfactant ratios using the 2018.3 version of the parallel MD simulation package GROMACS.[96,97] The LINCS algorithm[98] was employed to constrain all the bonds in the course of all four simulations, and the SETTLE algorithm[99] was also employed to constrain the water geometry of the rigid SPC/E model. The time-reversible simulation trajectory was generated by solving Newton's equation of motion using the leapfrog integrator. For neighbor list generation, the Verlet cutoff scheme was opted with a cutoff of 0.9 nm, and the frequency of the neighbor list was updated every 10 steps. A cutoff radius of 1.4 nm was used for the Lennard-Jones (LJ) interactions and standard long-range corrections. The particle mesh Ewald (PME) method[100,101] was employed to treat the long-range electrostatic interactions with fourth-order cubic interpolation and a Fourier spacing of 0.16 nm. We set the real space cutoff as 1.4 nm. In the *NVT* and *NPT* simulation runs, the temperature coupling was controlled via a velocity-rescaling thermostat[102,103] with a relaxation time of 0.5 ps. The modified Berendsen or velocity-rescaling thermostat contains an added stochastic term, which determines correct kinetic energy distribution, and a true canonical ensemble is generated.[102,103] However, the pressure coupling in the simulated systems was supplied by a Parrinello−Rahman barostat[104,105] with an isotropic coupling constant of 1.0 ps and a compressibility factor of 4.5×10^{-5} bar^{-1}. The simulation boxes were followed by the 3D periodic boundary conditions, with a simulation time step of 1 fs.

RESULTS AND DISCUSSION

Water Microstructure. *Triplet Angle Distributions.* The tetrahedral structure of normal bulk water may get altered by the effect of confinement[8,10,83] which influences the microscopic dynamics as well as the network of hydrogen bonds of water under confinement.[58−60,79] Recently, we have observed the unstructured tetrahedral network of water pools under strictly confined environments.[41] In the report, we have shown the restricted reorientation of water under strict confinements as compared with the confined one. In this work, the strictly confined environments are W_0 = 2 RM with n_{CTAB} = 28 and W_0 = 2 RM with n_{CTAB} = 40, and confined environments are W_0 = 5 RM with n_{CTAB} = 65 and W_0 = 10 RM with n_{CTAB} = 153. So, the slowing down of water reorientation may depend on the solution or surface confining the water. Local excluded volume is one such effect where the exchange of hydrogen-bonded partners is restricted and hence leads to slowing down of water reorientation.[106,107] The structural arrangement could also play such a role in hindering the exchange and reorientation of water in solution.[107−110] To detect the local packing or the structural order of hydrogen-bonded partners of water in the condensed phase, we have estimated the distribution of oxygen−oxygen−oxygen triplet angles using the following equation:[111]

$$P(\cos\theta_{OOO}) = \frac{1}{N \times (n_i - 2)} \left\langle \sum_{i=1}^{N} \sum_{j=1}^{n_i-1} \sum_{k=j+1}^{n_i} \delta\left(\cos\theta_{OOO} - \frac{r_{ij}\cdot r_{ik}}{|r_{ij}||r_{ik}|}\right) \right\rangle \quad (1)$$

Here, N is the number of molecules, n_i corresponds to the number of nearest neighbors present within the first coordination shell of molecule i, and r_{ij}, r_{ik} are vectors associated with the central molecule of its two nearest neighbors. This function measures the tetrahedrality of the system by calculating the angle between the vectors connecting the two nearest molecules with the central molecule.

In bulk water, this distribution was reported to exhibit a broad peak at 100° and a smaller peak at around 60°.[112] The two peaks correspond to the tetrahedral (100°)[107,112] and nontetrahedral (53°)[107,111] arrangement of liquid water. The broad peak near 100° also depicts the disordered state of the local tetrahedral network of liquid water as compared to the ice. In Figure 1, we have observed similar peaks at 100° and around 53°, which again diminish and shift with alteration of the strength of confinement. For comparison, we have included the distribution for bulk water molecules. It is important to note from Figure 1 the subtle diminishing of the tetrahedral

https://doi.org/10.1021/acs.jpcb.4c04773
J. Phys. Chem. B XXXX, XXX, XXX−XXX

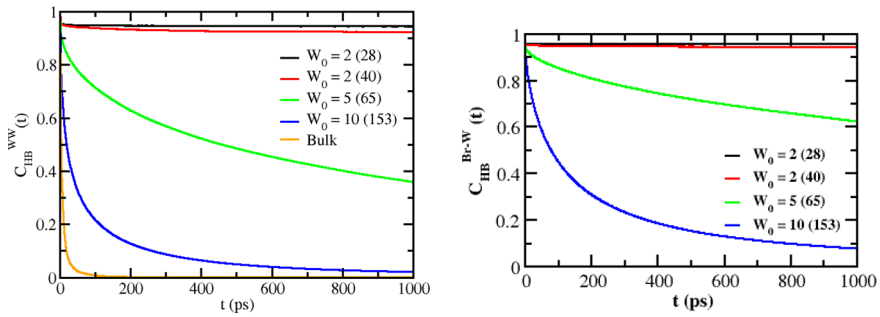

Figure 2. Intermittent hydrogen bond time correlation function, $C_{HB}(t)$, for (left) water···water and (right) Br^{-1}···water H-bonds present in the nanosize water pool for all four RM compositions (Table 1). The water···water H-bond for bulk water molecules is incorporated for comparison. Color code: black for W_0 = 2 RM with n_{CTAB} = 28; red for W_0 = 2 RM with n_{CTAB} = 40; green for W_0 = 5 RM with n_{CTAB} = 65; blue for W_0 = 10 RM with n_{CTAB} = 153; and orange for the bulk SPC/E water.

peak (100°) for the water pool confined inside RMs relative to bulk water. In W_0 = 2 with n_{CTAB} = 28 and W_0 = 2 with n_{CTAB} = 40, the tetrahedral peak (100°) in the distribution decreases and another peak at around 68° (W_0 = 2 with n_{CTAB} = 28) appears along with a shift of the nontetrahedral peak from 53° to angles even less than 50°. Interestingly, the tetrahedral peak (100°) reappears in the same state after increasing the water content inside the RMs (W_0 = 5 and W_0 = 10), depicting the formation of the tetrahedral structure of water after relaxing the effect of confinement. In a recent observation, we have estimated a higher value of the tetrahedral order parameter[113] for strictly confined environments (W_0 = 2 with n_{CTAB} = 28 and W_0 = 2 with n_{CTAB} = 40) suggesting the unstructured tetrahedral network of the water pool inside those RMs becomes ordered with increasing the water content (W_0 = 5 and W_0 = 10).[41] So, the above observations clearly indicate the influence of confinement on the tetrahedral structure of the nanoscale water pool.

Hydrogen Bond Distribution. The hydrogen bond (H-bond) plays a central role in maintaining the liquid water fluidity as well as the tetrahedral network, which is random in nature and rearranges constantly with breaking and formation of the H-bond. In liquid water, the fractional value of the H-bond signifies the presence of broken H-bonds in comparison to ice. So, the quantitative estimation of the number of H-bonds inside a confined environment can provide us with a qualitative picture of the water network. To investigate the same, we have computed the population of H-bonded states and the number of H-bonds per water molecule for four different RM compositions, based on geometric[1,4] criteria, and presented in Figure 1. In this report, we have considered purely geometric criteria to define a hydrogen bond, the water−water pair is treated to be hydrogen bonded, if the OW···OW distance is smaller than 0.35 nm and the OW···OW···HW1/HW2 angle is smaller than 30°.[4,114] The average number of H-bonds per water molecule was obtained using the formula:

$$\langle n_{HB} \rangle = \frac{N_{(\text{H-bonds})}}{N_{(\text{water-molecule})}} \quad (2)$$

where N corresponds to the number.

In Figure 1, we report the percentage of each hydrogen bonding state found in the water pool of RMs. In the inset of Figure 1, the number of hydrogen bonds per water molecule is incorporated. It is evident from Figure 1 that there is a decrease in the number of hydrogen bonds per water molecule as we move from bulk (unconstrained) to confined and strictly confined environments. Similar observations have been reported for the water confined near hydrophobic surfaces.[115,116] Djikaev and Ruckenstein have proposed a model to study the distance-dependent number of hydrogen bonds per water molecule near the hydrophobes.[115] Moreover, our observation indicates that the average number of H-bonds drops from 3.4 in the bulk to 0.6 inside the strict confinement of W_0 = 2 RM with n_{CTAB} = 28. This decrement could be attributed to the effect of confinement that restricts the space availability to form a regular tetrahedral water network in the aqueous pool of RMs, which is supported by the triplet angle distribution analysis (Figure 1), as discussed earlier. In such cases, the water molecules participate in the two hydrogen bonds (n_{HB} = 2) through the hydrogen atom, depicting the formation of a linear or quasi-2D water network in place of a regular tetrahedral arrangement. The absence of four coordinated (n_{HB} = 4) water molecules in W_0 = 2 RM with n_{CTAB} = 28 and 40 suggests the strong disruption of the water tetrahedral network in these reverse micellar systems. We have also noticed a considerable number of non-hydrogen-bonded (n_{HB} = 0) water molecules in extreme confinements, indicating the instability of the tetrahedral structure of water in such environments. It is interesting to note from Figure 1 that in the case of W_0 = 10 RM with n_{CTAB} = 153, the percentage of two (n_{HB} = 2) and three (n_{HB} = 3) coordinated hydrogen bonds is higher in nature followed up with a declining percentage of four (n_{HB} = 4) coordinated hydrogen bonds, which is larger in value for bulk. The percentage of single (n_{HB} = 1) and doubly (n_{HB} = 2) hydrogen-bonded molecules is higher in the case of W_0 = 5 RM with n_{CTAB} = 65. So, the hydrogen bond distribution analysis suggests the possibility of a quasi-2D network of the water pool in strict reverse micellar confinements; on the other hand, a rise of tetrahedrality is also noticed for higher order RMs (W_0 = 10 and W_0 = 5). In the bulk, the water network is tetrahedral in nature, and the percentage of hydrogen bonds obtained from our water SPC/E simulation is in close agreement with earlier reports.[107]

Hydrogen Bond Dynamics in the Nanoscale Water Pool. The nanoscale water network and the dynamics of water inside the interior of the RMs are highly influenced by the nature of the reverse micellar headgroup, counterions, and the essence of confinement. In the case of CTAB RMs, the headgroup methyl obstructs the formation of intermolecular hydrogen bonds with interfacial water confined inside RMs.[72] So, the hydrogen bond dynamics of water present in the interior of CTAB RMs are mostly influenced by the presence of a counterion (Br^{-1}) and the effect of confinement. The H-

https://doi.org/10.1021/acs.jpcb.4c04773
J. Phys. Chem. B XXXX, XXX, XXX−XXX

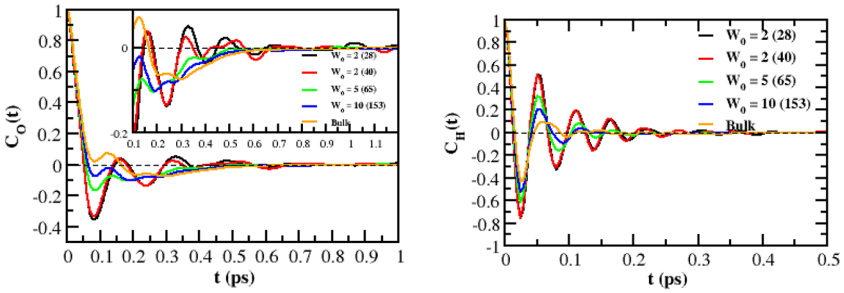

(a) (b)

Figure 3. (a) VACFs $C_v^O(t)$ for the oxygen atoms of water molecules present inside all four RMs (Table 1). The corresponding function for the hydrogen atoms $C_v^H(t)$ of the same state water are presented in (b). The VACFs for pure bulk water (SPC/E) are incorporated for comparison. Color code: black for W_0 = 2 with n_{CTAB} = 28; red for W_0 = 2 with n_{CTAB} = 40; green for W_0 = 5 with n_{CTAB} = 65; blue for W_0 = 10 with n_{CTAB} = 153; and orange for the bulk water.

bond can be defined as either an energetic[117] or a geometric[1,4,114] criterion. In the present work, we have opted for a geometric criterion to define a H-bond.[1,4,114]

To monitor the structural relaxation of water···water and Br^{-1}···water H-bonds present in the water pool, one can use the following time correlation function (TCF), defined as[118]

$$C_{HB}(t) = \langle h(0)h(t)\rangle/\langle h\rangle \quad (3)$$

Here, the dynamical variable $h(t)$ is equal to unity for the water···water or Br^{-1}···water site, which is hydrogen bonded at time t, and is zero otherwise. In the present work, we have optimized the geometric criteria to define a H-bond between the Br^{-1}···water pair, if the Br^{-1}···OW distance is smaller than 0.38 nm and the Br^{-1}···OW···HW1/HW2 angle is smaller than 30° (Figure S1), and the water···water pair H-bond criteria are already discussed in the previous section. The angular brackets depict the averaging over all pairs of water···water or Br^{-1}··· water H-bonds and over initial times. The $C_{HB}(t)$ indicates the probability that the H-bond between the water···water or Br^{-1}···water pair is intact at time t ($h(t) = 1$), given that it was intact at the initial time ($h(0) = 1$). So, the $C_{HB}(t)$ allows recrossing of the bonded and nonbonded states, and its relaxation gives information about the structural relaxation of a water···water or Br^{-1}···water H-bond pair.

We have computed the time correlation function $C_{HB}(t)$ for the H-bond formed between the water···water and Br^{-1}···water molecules present in the water pool for four different RM compositions (Table 1), and this is presented in Figure 2. The H-bond formed between a pair of bulk water molecules is incorporated for the purpose of comparison. The figure shows that the structural relaxation of water···water H-bonds present in the water pool for W_0 = 2 RM with n_{CTAB} = 28 and 40 is significantly slower than the other higher order RMs and in bulk water. Interestingly, the relaxation pattern shows an inhomogeneity in nature for water···water H-bonds for all four reverse micellar compositions. The structural relaxation behavior of the water···water H-bond pair clearly depicts the presence of slow components for all compositions that can be represented by multiexponentials.[1,4] However, the figure depicts the structural rearrangement of the nanoscale water pool network, along with its alteration with the effect of confinement. Importantly, the $C_{HB}^{WW}(t)$ relaxation shows a dependence on the confined environments, as we move from bulk to confined and strictly confined environments. Such confined environments influence the network of the water pool inside RMs. In the earlier sections, we have observed that the tetrahedral peak (100°) is completely missing for W_0 = 2 RM with n_{CTAB} = 28 and 40 (Figure 1), which reappears in the same state after increasing the water content in the RMs (W_0 = 5 and W_0 = 10). Further, the average number of H-bonds falls from 3.4 in the bulk to 0.6 for strict confinement, suggesting that the lack of space availability restricts the formation of a regular tetrahedral H-bond network in the water pool of RMs. Figure 1 shows the percentage of undercoordinated H-bonded water is higher for W_0 = 2 RM with n_{CTAB} = 28 and 40, whereas the higher order coordination of H-bonds is noticed in the case of higher order RMs as well as in the bulk. Interestingly, similar trends have been observed for Br^{-1}···water H-bonds. However, the Br^{-1}···water H-bonds show much slower relaxation as compared to the water···water H-bonds. In the recent past, Chandra has observed that the anion···water H-bond relaxation behavior is slower with respect to the water···water H-bonds.[119] In another study, Dokter et al. have shown that the water molecules present in the Br^{-1} anion-rich CTAB interfacial region are more rigid as compared to the bulk water.[48] So, our observation shows a close association with previous reports.

The above observation can assist in explaining the differential nature of $C_{HB}^{WW}(t)$ relaxation. The breaking and formation of water···water H-bonds are highly concerted processes, and $C_{HB}^{WW}(t)$ allows reformation of broken H-bonds.[1] Particularly, it allows recrossing of the bonded and nonbonded states. The recrossing of H-bonds occurs quickly in the case of highly coordinated H-bonded water, whereas the undercoordinated case shows low proximity of switching H-bonds and slows down the recrossing process. The slowest relaxation of $C_{HB}^{WW}(t)$ for W_0 = 2 with n_{CTAB} = 28 and 40 resembles the low probability of switching H-bonds from one H-bonded site to another H-bonded site, may slow down the recrossing as well as the relaxation, and is correlated with restricted reorientation under strict confinement, as reported separately.[41] On the other hand, the water content increases inside the RMs supporting the formation of higher order H-bond coordination with quicker recrossing behavior, which influences the faster decay for higher order RMs (W_0 = 5 and W_0 = 10) as well as in bulk water. So, the above observations agree well with the lowering trends of tetrahedral ordering of the nanoscale water pool inside RMs, as we move from bulk to confined and strictly confined environments, which is in consonance with slower $C_{HB}^{WW}(t)$ relaxation and restricted

https://doi.org/10.1021/acs.jpcb.4c04773
J. Phys. Chem. B XXXX, XXX, XXX−XXX

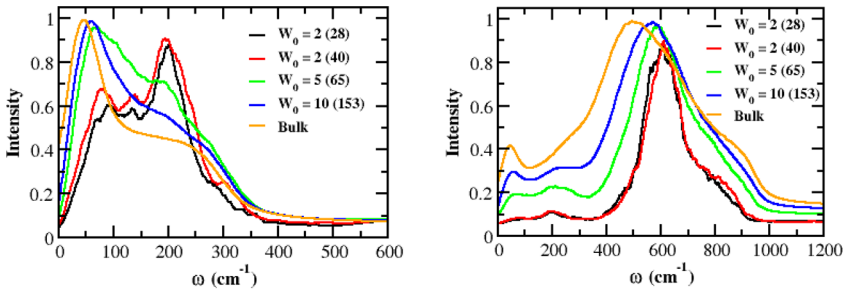

Figure 4. (a) Power spectra $S_O(\omega)$ for the oxygen atoms of water molecules present inside all four RMs (Table 1). The corresponding power spectra for the hydrogen atoms $S_H(\omega)$ of the same state water are displayed in (b). The power spectrum for pure bulk water (SPC/E) is incorporated for comparison. Color code: black for W_0 = 2 RM with n_{CTAB} = 28; red for W_0 = 2 RM with n_{CTAB} = 40; green for W_0 = 5 RM with n_{CTAB} = 65; blue for W_0 = 10 RM with n_{CTAB} = 153; and orange for the bulk SPC/E water.

reorientation[41] of the water pool in W_0 = 2 RM with n_{CTAB} = 28 and 40, supporting the effect of confinement on the tetrahedral structure of the water pool network.

Velocity Autocorrelation Function in the Nanoscale Water Pool. The dynamics of a nanoscale water pool confined inside CTAB RMs of varied $W_0 = [H_2O]/[CTAB]$ ratios can be estimated by various other time correlation functions and the corresponding spectral densities. The density of states (DOS) is associated with different dynamical behavior. In this report, we have computed the velocity autocorrelation function (VACF) along with its Fourier transformation that can provide us with the low-frequency intermolecular vibrational density of states of the water pool confined inside RMs. The VACF can be defined as

$$C_v^i(t) = \frac{\langle v(t)\cdot v(0)\rangle}{\langle v(0)\cdot v(0)\rangle} \tag{4}$$

where $\vec{v}(t)$ is the velocity of the i_{th} atom (O or H) of the water molecule under study at time t and the angular brackets represent averaging over all molecules considered for the VACF and over initial times. The VACF gives an average description of the collisions between atoms in a system. Collisions change the direction and magnitude of atomic velocities, and after a few collisions, correlations between the initial velocity of an atom and the velocity at a later time may be lost. The Fourier transformation of the VACF to a vibrational density of states generated from MD simulation is a common approach.[83]

The VACFs for oxygen (C_v^O) and hydrogen (C_v^H) atoms of water present in RMs were calculated separately and are displayed in Figure 3. For comparison, we have incorporated the bulk separately for individual figures.

Figure 3 shows a significant difference in the relaxation behavior of $C_v^O(t)$ and $C_v^H(t)$ for the four different RMs with varied $W_0 = [H_2O]/[CTAB]$ ratios and bulk water. The $C_v^O(t)$ function for the bulk water exhibits an initial small bump followed by a dip. The small positive bump before negative minima in the VACF appears due to the longitudinal components as studied by Balucani et al.[120] This positive bump occurs close to 0.085 ps for all four reverse micellar systems including bulk and shifts to more negative values for water confined inside CTAB RMs, as we move from bulk to confined and strictly confined environments. However, the shift for the W_0 = 2 RM with n_{CTAB} = 28 system is more negative followed up with W_0 = 2 RM with n_{CTAB} = 40, W_0 = 5 with n_{CTAB} = 65, and W_0 = 10 with n_{CTAB} = 153, which is decreasing in order. The first minimum occurs because of the "caging effect", which arises from backscattering of water oxygen atoms due to collisions with neighboring molecules forming cages around them.[83] The deeper minimum suggests enhanced rigidity of the nanoscale water pool with more strong confinement. Interestingly, for bulk water, the VACF decays within 0.6 ps, whereas water confined inside the CTAB RM, specifically W_0 = 2 with n_{CTAB} = 28 and W_0 = 2 with n_{CTAB} = 40, rather shows oscillating behavior and does not decay entirely to zero at long times. Similar behavior of water motions has been reported for water confined in biological systems as well.[121] In addition, a distinct broadening of the first minimum and a systematic shift of the second minima appearing ~0.2 ps for bulk water to values greater than 0.2 ps indicate strong distortion of the tetrahedral network of water confined inside the W_0 = 2 RM with n_{CTAB} = 28 and 40. Further, the motions of water molecules in W_0 = 2 with n_{CTAB} = 28 and 40 RMs are more correlated in comparison with W_0 = 5 RM with n_{CTAB} = 65 and W_0 = 10 RM with n_{CTAB} = 153 along with bulk water. The broad conclusions drawn from the $C_v^O(t)$ function are underpinned by an examination of the $C_v^H(t)$ function, focusing on hydrogen atoms of water confined inside the CTAB RM, as illustrated in Figure 3. Due to the small mass, the $C_v^H(t)$ decays much faster in the case of bulk water with the amplitude vanishing in less than 0.2 ps time. Moreover, the $C_v^H(t)$ provides information about the librational motions (hindered rotations) of water molecules, and the general oscillatory nature of the function with a significantly deeper minimum indicates stronger caging effects on water liberation. Our calculations suggest that the librational motions of water inside W_0 = 2 RM with n_{CTAB} = 28 and 40 are hindered to a greater extent followed up with W_0 = 5 RM with n_{CTAB} = 65 and W_0 = 10 RM with n_{CTAB} = 153, which is decreasing in order with the increase of reverse micellar aqueous pool. This supports the restricted reorientation of water molecules inside the strictly confined environment (W_0 = 2 RM with n_{CTAB} = 28 and 40), which is relaxed with the addition of water content inside RMs (W_0 = 5 RM with n_{CTAB} = 65 and W_0 = 10 RM with n_{CTAB} = 153).[41] Again, the W_0 = 2 RM with n_{CTAB} = 28 and 40 shows strong oscillatory motion, which gradually fades away with the relaxation in confinement or increase of reverse micellar size. The differential influence of confinement on the VACF of the nanoscale water pool may

https://doi.org/10.1021/acs.jpcb.4c04773
J. Phys. Chem. B XXXX, XXX, XXX−XXX

alter the low-frequency intermolecular vibrational spectrum of the water in RMs.

Vibrational Spectrum of the Nanoscale Water Pool. Several experiments[122−124] and simulation studies[83,125] have shown two broad low-frequency vibrational bands present in water, one at 50 cm^{-1} and the other at 200 cm^{-1}. Importantly, the band around 50 cm^{-1} corresponds to the O···O···O triplet bending mode of H-bonded water, and the band around 200 cm^{-1} depicts the O···O stretching mode between water···water H-bonded pairs. However, there is uncertainty in the interpretation of the 50 cm^{-1} band. Marti et al. have shown that the 50 cm^{-1} band is not indispensable for H-bonded liquids, and the band can be observed for non-H-bonded liquids.[125] Importantly, the origin of the 50 cm^{-1} band may be from restricted transverse translations of molecular triplets, and the addition of H-bonds in such triplets may alter the position of this band.

It is clear from the above discussion that the H-bonds in liquid water can play a vital role in determining the low-frequency vibrational bands. In the previous sections, we have presented the effect of confinement on the tetrahedral structure of the water network that makes an impact on the low-frequency band of nanoscale water pools confined inside RMs (Table 1). To observe this fact, we have computed the power spectra $S_O(\omega)$ and $S_H(\omega)$ of water molecules by a Fourier cosine transform of the velocity auto time correlation functions for the oxygen and hydrogen atoms, which are displayed in Figure 4.

In Figure 4, we have presented the power spectra $S_O(\omega)$ for the oxygen atoms of the nanoscale water pool inside four different RMs (Table 1) along with pure bulk (SPC/E) water. It is clear from the figure that relative to bulk water, we observed a blue shift by ∼18−45 cm^{-1} in the frequency occurring at 50 cm^{-1}, corresponding to the O···O···O bending mode of the H-bonded water molecules or restricted translations of molecular triplets inside the molecular cages for water in the RMs. The blue shift for more confined systems tends to induce restricted translations of the nanoscale water pool at higher frequencies. However, the addition of water content inside the RMs brings the propensity of the band position toward the bulk value. In $S_O(\omega)$, the intensity of the 50 cm^{-1} band drops from bulk to confined and strictly confined environments, depicting the reduced tendency of molecular triplet (O···O···O) formation, which is an integral part of the construction of the water tetrahedral structure. In the case of strict confinements, our earlier observations indicate the missing tetrahedral peak ∼100° (Figure 1) and the absence of higher coordinated H-bonded water molecules as well as the large percentage of undercoordinated H-bonded water (Figure 1), which support the formation of a quasi-two-dimensional water network and the depletion of O···O···O triplet formation in W_0 = 2 RM with n_{CTAB} = 28 and 40. In the recent past, several research groups have shown that the alteration of the 50 cm^{-1} band is closely connected to the rigidity of the water network in confined surfaces.[82,83] The position of the O···O stretching or longitudinal translation band at ∼200 cm^{-1} is not influenced much by the confinement effect. This is an interesting observation, depicting that reverse micellar confinement has minimal effect on the local motions, which are key contributors to such a low-frequency vibrational band. Moreover, a significant intensity variation at the ∼200 cm^{-1} band depicts the impact of confinement on the tetrahedral ordering of the nanoscale water pool in the RMs. The higher intensity for strictly confined environments, in this study, the W_0 = 2 RM with n_{CTAB} = 28 and 40 are considered as the strict confinement, are influencing the tetrahedral water structure to adopt the quasi-two-dimensional structure and exhibit restricted longitudinal translations responsible for higher intensity under strong confinements, while this condition is relaxed after increasing the water content inside the RMs and the band intensity is converged toward bulk value. Marti and co-workers[82] have shown the formation of a quasi-2D water structure under strong graphitic confinements. The librational band of water inside reverse micellar confinement has also been observed to be affected significantly, as noticed from the power spectrum of hydrogen atom $S_H(\omega)$, and is presented in Figure 4. It is noticed from the figure that the librational band at ∼500 cm^{-1} for unconstrained bulk water (SPC/E) has been found to be blue-shifted by ∼71−112 cm^{-1} for the water pool in RMs (Table 1). The appearance of a ∼612 cm^{-1} peak for W_0 = 2 RM with n_{CTAB} = 28 and 40 clearly signifies that reverse micellar confinement restricts the librational motion of the nanoscale water pool and alters its tetrahedral ordering, supporting the hindered reorientation of water inside the strict confinement.[41] Furthermore, the results presented in this section are in good agreement with the MD simulation studies of water under various graphitic confinements.[82]

CONCLUSIONS

In this work, we have investigated in detail the effect of confinement on microscopic dynamics and spectroscopy of nanoscale water pools inside RMs. To conduct this investigation, we have performed classical MD simulations of four different CTAB/water/chloroform RMs with varied water content, and the detailed composition of the systems is presented in Table 1. The bulk water (SPC/E) simulation was conducted separately for the purpose of comparison. In this work, we made an attempt to explore how the tetrahedral ordering of nanoscale water inside reverse micellar confinement influences the microscopic dynamics and the structural relaxation of water···water H-bonds and its impact on the low-frequency intermolecular vibrational band of the same state water.

In our study, we have observed that the tetrahedral peak ∼100° is completely missing in the case of strict confinements (Figure 1). The W_0 = 2 RM with n_{CTAB} = 28 and 40 are considered as strict confinements. Interestingly, the missing peak reappears in the same state after increasing the water content inside the RMs. Further, we have noticed a depletion in the number of H-bonds per water molecule as we move from bulk (unconstrained) to confined and strictly confined environments (Figure 1). This indicates that the confinement restricts the space availability to form a regular tetrahedral water network in the aqueous pool of RMs. In such a strict environment, the water molecules mostly participate in the two H-bonds through hydrogen atoms, indicating the formation of a linear or quasi-two-dimensional water network in place of a regular tetrahedral arrangement. This proposition is partly supported by the evidence of missing tetrahedral peaks, the absence of higher coordinated water molecules, and the presence of a large percentage of undercoordinated water for strict reverse micellar confinement. The structural relaxation of water···water H-bonds present in the nanoscale water pool of RMs is significantly altered as per the order of confinement. The relaxation behavior clearly depicts the presence of slow

https://doi.org/10.1021/acs.jpcb.4c04773
J. Phys. Chem. B XXXX, XXX, XXX−XXX

components, which can be explained by the fitting of the multiexponential law. Importantly, the $C_{HB}^{WW}(t)$ relaxation also revealed a dependence on the order of confined environments, as we shift from bulk to confined and strictly confined environments. In this work, we have presented an explanation related to the recrossing of hydrogen bonds, which can play a vital role in explaining the relaxation pattern of $C_{HB}^{WW}(t)$ under confinement. So, the results clearly indicate the decreasing trends of tetrahedral ordering of water pools in reverse micellar confinements, as we move from bulk to confined and strictly confined environments. In addition, a similar trend of H-bond relaxation has been observed for Br^{-1}···water H-bonds, which shows a much slower relaxation as compared to the water··· water H-bonds.

The blue shift by ∼18−45 cm^{-1} is observed in the low-frequency O···O···O band occurring at 50 cm^{-1} of the H-bonded water molecules or restricted translations of molecular triplets inside the molecular cages for water in the RMs. Further, the more confined systems tend to induce larger restrictions during the translation of nanoscale water pools and shift the frequency to a higher value. However, the addition of water in the RMs brings the band toward the bulk. In addition, the intensity of the 50 cm^{-1} band drops from bulk to confined and strictly confined environments, indicating the reduced tendency of molecular triplet (O···O···O) formation. The molecular triplets (O···O···O) are an integral part of the water tetrahedral structure. Consistent with our earlier observation, we have shown that strict confinement influences the formation of a quasi-two-dimensional water network in place of a tetrahedral water structure, which is the key factor for the missing tetrahedral peak and absence of higher coordinated H-bonded water, supporting the depletion of water tetrahedral ordering and restricting its translation under a strict environment. To the best of our knowledge, this is the first such work where it is explored that the impact of reverse micellar confinement on the tetrahedral ordering of the nanoscale water pool and the microscopic dynamics as well as the structural relaxation of water···water hydrogen bonds are correlated with the alteration of the 50 cm^{-1} low-frequency band for water inside RMs. Using various spectroscopic techniques, such as 2D-IR, THz, and Raman experiments, one can verify these microscopic correlations. So, the mentioned experiments in association with simulation studies can provide a detailed microscopic picture of water under various complex confinements.

The position of the O···O stretching or longitudinal translation band appearing at ∼200 cm^{-1} is unaffected by the confinement effect. This is an important observation, indicating that reverse micellar confinement has minimal effect on the local motions and is a primary contributor to the ∼200 cm^{-1} band. Further, a significant intensity variation at the 200 cm^{-1} band indicates the effect of confinement on the tetrahedral ordering of the water pool inside the RMs. Surprisingly, the higher intensity for strictly confined environments supports its influence on the tetrahedral water structure to adopt the quasi-two-dimensional structure and experience restricted longitudinal translations. Further, the addition of water inside RMs can reinstate the tetrahedral network of water and restore the ∼200 cm^{-1} band intensity toward the bulk value. In the recent past, Marti and co-workers[82] have also shown the formation of such a quasi-2D water structure under graphitic confinements.

The librational band occurring at ∼500 cm^{-1} for water under reverse micellar confinement is found to be blue-shifted by ∼71−112 cm^{-1}. Interestingly, the appearance of the ∼612 cm^{-1} band for a strictly confined environment clearly signifies the confinement effect that restricts the librational motion of nanoscale water pools and alters the water tetrahedral ordering. Further, it would be very promising to correlate the librational motion with the reorientational dynamics of the nanoscale water pool inside the RMs. Presently, we are working on such interesting investigations under various complex confinements.

■ ASSOCIATED CONTENT

Supporting Information

The Supporting Information is available free of charge at https://pubs.acs.org/doi/10.1021/acs.jpcb.4c04773.

Additional details regarding the Br^{-1}···water hydrogen bond (PDF)

■ AUTHOR INFORMATION

Corresponding Author

Sudip Chakraborty − *Department of Computational Sciences, School of Basic Sciences, Central University of Punjab, Bathinda 151401, India;* orcid.org/0009-0008-5104-4907; Email: sudip.chakraborty@cup.edu.in

Authors

Anupama Sharma − *Department of Computational Sciences, School of Basic Sciences, Central University of Punjab, Bathinda 151401, India*

Mywish Anand − *Department of Computational Sciences, School of Basic Sciences, Central University of Punjab, Bathinda 151401, India;* orcid.org/0000-0003-3430-091X

Complete contact information is available at: https://pubs.acs.org/10.1021/acs.jpcb.4c04773

Notes

The authors declare no competing financial interest.

■ ACKNOWLEDGMENTS

This work was supported in part by generous grants from the University Grants Commission (UGC)—BSR Start-up grant (F.30-432/2018(BSR)), Central University of Punjab—Research Seed Money, Department of Science and Technology (DST) under Fast Track Scheme for Young Scientist (SB/FT/CS-158/2013), Government of India. A.S. thanks CSIR for providing a scholarship. S.C. is thankful to Prof. Raghavendra P. Tiwari, Vice Chancellor, Central University of Punjab Bathinda, for encouraging the research and providing the necessary facilities.

■ DEDICATION

This article is dedicated to the memory of Prof. Branka Maria Ladanyi.

■ REFERENCES

(1) Bandyopadhyay, S.; Chakraborty, S.; Bagchi, B. Secondary structure sensitivity of hydrogen bond lifetime dynamics in the protein hydration layer. *J. Am. Chem. Soc.* **2005**, *127*, 16660−16667.
(2) Bandyopadhyay, S.; Chakraborty, S.; Balasubramanian, S.; Bagchi, B. Sensitivity of Polar Solvation Dynamics to the Secondary

Structures of Aqueous Proteins and the Role of Surface Exposure of the Probe. *J. Am. Chem. Soc.* **2005**, *127*, 4071−4075.
(3) Gertner, B. J.; Whitnell, R. M.; Wilson, K. R.; Hynes, J. T. Activation to the transition state: Reactant and solvent energy flow for a model SN2 reaction in water. *J. Am. Chem. Soc.* **1991**, *113*, 74−87.
(4) Sharma, A.; Kumar, V.; Chakraborty, S. Micro-Solvation of Propofol in Propylene Glycol−Water Binary Mixtures: Molecular Dynamics Simulation Studies. *J. Phys. Chem. B* **2023**, *127*, 11011−11022.
(5) Peter, C.; Hummer, G. Ion transport through membrane-spanning nanopores studied by molecular dynamics simulations and continuum electrostatics calculations. *Biophysical journal* **2005**, *89*, 2222−2234.
(6) Singer, S. J.; Nicolson, G. L. The Fluid Mosaic Model of the Structure of Cell Membranes. *Science* **1972**, *175*, 720−731.
(7) Ball, P. Water as an Active Constituent in Cell Biology. *Chem. Rev.* **2008**, *108*, 74−108.
(8) Coudert, F.-X.; Vuilleumier, R.; Boutin, A. Dipole Moment, Hydrogen Bonding and IR Spectrum of Confined Water. *ChemPhysChem* **2006**, *7*, 2464−2467.
(9) da Silva, L. B. Structural and dynamical properties of water confined in carbon nanotubes. *J. Nanostruct. Chem.* **2014**, *4*, 104.
(10) Chakraborty, S.; Kumar, H.; Dasgupta, C.; Maiti, P. K. Confined Water: Structure, Dynamics, and Thermodynamics. *Acc. Chem. Res.* **2017**, *50*, 2139−2146.
(11) Head-Gordon, T.; Johnson, M. E. Tetrahedral structure or chains for liquid water. *Proc. Natl. Acad. Sci. U.S.A* **2006**, *103*, 7973−7977.
(12) Bai, J.; Zeng, X. C. Polymorphism and polyamorphism in bilayer water confined to slit nanopore under high pressure. *Proc. Natl. Acad. Sci. U. S. A.* **2012**, *109*, 21240−21245.
(13) Jinesh, K. B.; Frenken, J. W. M. Experimental evidence for ice formation at room temperature. *Phys. Rev. Lett.* **2008**, *101*, No. 036101.
(14) Giovambattista, N.; Rossky, P. J.; Debenedetti, P. G. Effect of pressure on the phase behavior and structure of water confined between nanoscale hydrophobic and hydrophilic plates. *Phys. Rev. E* **2006**, *73*, No. 041604.
(15) Bagchi, B. Water dynamics in the hydration layer around proteins and micelles. *Chem. Rev.* **2005**, *105*, 3197−3219.
(16) Holt, J. J.; Park, H. G.; Wang, Y.; Stadermann, M.; Artyukhin, A. B.; Grigoropoulos, C. P.; Noy, A.; Bakajin, O. Fast mass transport through sub-2-nanometer carbon nanotubes. *Science* **2006**, *312*, 1034−1037.
(17) Mukherjee, B.; Maiti, P. K.; Dasgupta, C.; Sood, A. K. Jump reorientation of water molecules confined in narrow carbon nanotubes. *J. Phys. Chem. B* **2009**, *113*, 10322−10330.
(18) Levinger, N. E. Water in Confinement. *Science* **2002**, *298*, 1722−1723.
(19) Moilanen, D. E.; Fenn, E. E.; Wong, D.; Fayer, M. D. Water dynamics in large and small reverse micelles: From two ensembles to collective behavior. *J. Chem. Phys.* **2009**, *131*, No. 014704.
(20) Dinh, T. D.; Phan, M. N.; Nguyen, D. T.; Le, T. M. D.; Nadda, A. K.; Srivastav, A. L.; Pham, T. N. M.; Pham, T. D. Removal of beta-lactam antibiotic in water environment by adsorption technique using cationic surfactant functionalized nanosilica rice husk. *Environmental Research* **2022**, *210*, No. 112943.
(21) Mora, A. K.; Singh, P. K.; Nadkarni, S. A.; Nath, S. How mobile is the water in the reverse micelles? A 2DIR study with an ultrasmall IR probe. *J. Mol. Liq.* **2021**, *327*, No. 114819.
(22) van der Loop, T. H.; Panman, M. R.; Lotze, S.; Zhang, J.; Vad, T.; Bakker, H. J.; Sager, W. F.; Woutersen, S. Structure and dynamics of water in nonionic reverse micelles: A combined time-resolved infrared and small angle x-ray scattering study. *J. Chem. Phys.* **2012**, *137*, No. 044503.
(23) Honegger, P.; Steinhauser, O. Revival of collective water structure and dynamics in reverse micelles brought about by protein encapsulation. *Phys. Chem. Chem. Phys.* **2018**, *20*, 22932−22945.
(24) Patra, A.; Luong, T. Q.; Mitra, R. K.; Havenith, M. The influence of charge on the structure and dynamics of water encapsulated in reverse micelles. *Phys. Chem. Chem. Phys.* **2014**, *16*, 12875−12883.
(25) Khoshnood, A.; Firoozabadi, A. Polar solvents trigger formation of reverse micelles. *Langmuir* **2015**, *31*, 5982−5991.
(26) Chowdhary, J.; Ladanyi, B. M. Molecular dynamics simulation of aerosol-OT reverse micelles. *J. Phys. Chem. B* **2009**, *113*, 15029−15039.
(27) Chakraborty, T.; Chakraborty, I.; Ghosh, S. The methods of determination of critical micellar concentrations of the amphiphilic systems in aqueous medium. *Arabian Journal of Chemistry* **2011**, *4*, 265−270.
(28) Chen, Y.; Liu, Y.; Yao, Y.; Zhang, S.; Gu, Z. Reverse micelle-based water-soluble nanoparticles for simultaneous bioimaging and drug delivery. *Org. Biomol. Chem.* **2017**, *15*, 3232−3238.
(29) Nicot, C.; Vacher, M.; Vincent, M.; Gallay, J.; Waks, M. Membrane proteins as reverse micelles: Myelin basic protein in a membrane-mimetic environment. *Biochemistry* **1985**, *24*, 7024−7032.
(30) Marhuenda-Egea, F. C.; Piera-Velázquez, S.; Cadenas, C.; Cadenas, E.; et al. Reverse micelles in organic solvents: a medium for the biotechnological use of extreme halophilic enzymes at low salt concentration. *Archaea* **2002**, *1*, 105−111.
(31) Senske, M.; Xu, Y.; Bäumer, A.; Schäfer, S.; Wirtz, H.; Savolainen, J.; Weingärtner, H.; Havenith, M. Local chemistry of the surfactant's head groups determines protein stability in reverse micelles. *Phys. Chem. Chem. Phys.* **2018**, *20*, 8515−8522.
(32) Melo, E. P.; Aires-Barros, M. R.; Cabral, J. M. S. Reverse micelles and protein biotechnology. *Biotechnology Annual Review* **2001**, *7*, 87−129.
(33) Mohyaldinn, M. E.; Alakbari, F. S.; Bin Azman Nor, A. N. A.; Hassan, A. M. Stability, Rheological Behavior, and pH Responsiveness of CTAB/HCl Acidic Emulsion: Experimental Investigation. *ACS Omega* **2023**, *8*, 22428−22439.
(34) Sankar, K. A.; Kumar, C. S.; Mohanta, K. Highly Stable Aqueous Dispersion of CTAB-Intercalated Reduced Graphene Oxide. *Mater. Today: Proc.* **2019**, *18*, 759−764.
(35) Liu, Y.; Tourbin, M.; Lachaize, S.; Guiraud, P. Silica nanoparticles separation from water: Aggregation by cetyltrimethylammonium bromide (CTAB). *Chemosphere* **2013**, *92*, 681−687.
(36) Padalkar, S.; Capadona, J. R.; Rowan, S. J.; Weder, C.; Won, Y.-H.; Stanciu, L. A.; Moon, R. J. Natural biopolymers: novel templates for the synthesis of nanostructures. *Langmuir* **2010**, *26*, 8497−8502.
(37) Hossain, S.; Kabedev, A.; Parrow, A.; Bergstrom, C. A.; Larsson, P. Molecular simulation as a computational pharmaceutics tool to predict drug solubility, solubilization processes and partitioning. *Eur. J. Pharm. Biopharm.* **2019**, *137*, 46−55.
(38) Kuznetsova, D. A.; Vasilieva, E. A.; Kuznetsov, D. M.; Lenina, O. A.; Filippov, S. K.; Petrov, K. A.; Zakharova, L. Y.; Sinyashin, O. G. Enhancement of the transdermal delivery of nonsteroidal anti-inflammatory drugs using liposomes containing cationic surfactants. *ACS omega* **2022**, *7*, 25741−25750.
(39) Pawar, S. S.; Iyyaswami, R.; Belur, P. D. Reverse micellar extraction of lactoferrin from its synthetic solution using CTAB/n-heptanol system. *Journal of food science and technology* **2017**, *54*, 3630−3639.
(40) Swami, A.; Kumar, A.; Sastry, M. Formation of water-dispersible gold nanoparticles using a technique based on surface-bound interdigitated bilayers. *Langmuir* **2003**, *19*, 1168−1172.
(41) Anand, M.; Chakraborty, S. In-Silico Investigation of Confined Water Dynamics in CTAB/Water/Chloroform Reverse Micelles. *Submitted*.
(42) Ranjan, R.; Vaidya, S.; Thaplyal, P.; Qamar, M.; Ahmed, J.; Ganguli, A. K. Controlling the size, morphology, and aspect ratio of nanostructures using reverse micelles: a case study of copper oxalate monohydrate. *Langmuir* **2009**, *25*, 6469−6475.
(43) Lin, X.; Sorensen, C.; Klabunde, K.; Hadjipanayis, G. Temperature dependence of morphology and magnetic properties

https://doi.org/10.1021/acs.jpcb.4c04773
J. Phys. Chem. B XXXX, XXX, XXX−XXX

of cobalt nanoparticles prepared by an inverse micelle technique. *Langmuir* **1998**, *14*, 7140−7146.
(44) Faeder, J.; Ladanyi, B. Molecular dynamics simulations of the interior of aqueous reverse micelles. *J. Phys. Chem. B* **2000**, *104*, 1033−1046.
(45) Zulauf, M.; Eicke, H. F. Inverted micelles and microemulsions in the ternary system water/aerosol-OT/isooctane as studied by photon correlation spectroscopy. *J. Phys. Chem.* **1979**, *83*, 480−486.
(46) Balakrishnan, S.; Javid, N.; Weingärtner, H.; Winter, R. Small-Angle X-Ray Scattering and Near-Infrared Vibrational Spectroscopy of Water Confined in Aerosol-OT Reverse Micelles. *ChemPhysChem* **2008**, *9*, 2794−2801.
(47) Abel, S.; Sterpone, F.; Bandyopadhyay, S.; Marchi, M. Molecular Modeling and Simulations of AOT-Water Reverse Micelles in Isooctane: Structural and Dynamic Properties. *J. Phys. Chem. B* **2004**, *108*, 19458−19466.
(48) Dokter, A. M.; Woutersen, S.; Bakker, H. J. Ultrafast dynamics of water in cationic micelles. *J. Chem. Phys.* **2007**, *126*, 124507.
(49) Dokter, A. M.; Woutersen, S.; Bakker, H. J. Inhomogeneous dynamics in confined water nanodroplets. *Proc. Natl. Acad. Sci. U. S. A.* **2006**, *103*, 15355−15358.
(50) Cringus, D.; Bakulin, A.; Lindner, J.; Vohringer, P.; Pshenichnikov, M. S.; Wiersma, D. A. Ultrafast Energy Transfer in Water-AOT Reverse Micelles. *J. Phys. Chem. B* **2007**, *111*, 14193−14207.
(51) Piletic, I. R.; Moilanen, D. E.; Spry, D.; Levinger, N. E.; Fayer, M. Testing the core/shell model of nanoconfined water in reverse micelles using linear and nonlinear IR spectroscopy. *J. Phys. Chem. A* **2006**, *110*, 4985−4999.
(52) Costard, R.; Levinger, N. E.; Nibbering, E. T. J.; Elsaesser, T. Ultrafast Vibrational Dynamics of Water Confined in Phospholipid Reverse Micelles. *J. Phys. Chem. B* **2012**, *116*, 5752−5759.
(53) Mondal, S. K.; Ghosh, S.; Sahu, K.; Mandal, U.; Bhattacharyya, K. Ultrafast fluorescence resonance energy transfer in a reverse micelle: Excitation wavelength dependence. *J. Chem. Phys.* **2006**, *125*, 224710.
(54) Cringus, D.; Lindner, J.; Milder, M. T.; Pshenichnikov, M. S.; Vohringer, P.; Wiersma, D. A. Femtosecond water dynamics in reverse-micellar nanodroplets. *Chem. Phys. Lett.* **2005**, *408*, 162−168.
(55) Loparo, J. J.; Roberts, S. T.; Tokmakoff, A. Multidimensional infrared spectroscopy of water. I. Vibrational dynamics in two-dimensional IR line shapes. *J. Chem. Phys.* **2006**, *125*, 194521.
(56) Asbury, J. B.; Steinel, T.; Stromberg, C.; Corcelli, S. A.; Lawrence, C. P.; Skinner, J. L.; Fayer, M. D. Water Dynamics: Vibrational Echo Correlation Spectroscopy and Comparison to Molecular Dynamics Simulations. *J. Phys. Chem. A* **2004**, *108*, 1107−1119.
(57) Kraemer, D.; Cowan, M. L.; Paarmann, A.; Huse, N.; Nibbering, E. T. J.; Elsaesser, T.; Miller, R. J. D. Temperature dependence of the two-dimensional infrared spectrum of liquid H2O. *Proc. Natl. Acad. Sci. U. S. A.* **2008**, *105*, 437−442.
(58) Piletic, I. R.; Tan, H. S.; Fayer, M. D. Dynamics of Nanoscopic Water: Vibrational Echo and Infrared Pump-Probe Studies of Reverse Micelles. *J. Phys. Chem. B* **2005**, *109*, 21273−21284.
(59) Gilijamse, J. J.; Lock, A. J.; Bakker, H. J. Dynamics of confined water molecules. *Proc. Natl. Acad. Sci. U. S. A.* **2005**, *102*, 3202−3207.
(60) Kumar, S. K. K.; Tamimi, A.; Fayer, M. D. Dynamics in the Interior of AOT Lamellae Investigated with Two-Dimensional Infrared Spectroscopy. *J. Am. Chem. Soc.* **2013**, *135*, 5118−5126.
(61) Angulo, G.; Organero, J. A.; Carranza, M.; Douhal, A. Probing the behavior of confined water by proton-transfer reactions. *J. Phys. Chem. B* **2006**, *110*, 24231−24237.
(62) Klicova, L.; Muchová, E.; Sebej, P.; Slavicek, P.; Klán, P. Nature of CTAB/water/chloroform reverse micelles at above-and subzero temperatures studied by NMR and molecular dynamics simulations. *Langmuir* **2015**, *31*, 8284−8293.
(63) Rosenfeld, D. E.; Schmuttenmaer, C. A. Dynamics of the water hydrogen bond network at ionic, nonionic, and hydrophobic interfaces in nanopores and reverse micelles. *J. Phys. Chem. B* **2011**, *115*, 1021−1031.
(64) Faeder, J.; Albert, M. V.; Ladanyi, B. M. Molecular dynamics simulations of the interior of aqueous reverse micelles: A comparison between sodium and potassium counterions. *Langmuir* **2003**, *19*, 2514−2520.
(65) Faeder, J.; Ladanyi, B. M. Solvation dynamics in aqueous reverse micelles: a computer simulation study. *J. Phys. Chem. B* **2001**, *105*, 11148−11158.
(66) Onori, G.; Santucci, A. IR investigations of water structure in Aerosol OT reverse micellar aggregates. *J. Phys. Chem.* **1993**, *97*, 5430−5434.
(67) Pieniazek, P. A.; Lin, Y.-S.; Chowdhary, J.; Ladanyi, B. M.; Skinner, J. Vibrational spectroscopy and dynamics of water confined inside reverse micelles. *J. Phys. Chem. B* **2009**, *113*, 15017−15028.
(68) Villa, C. C.; Correa, N. M.; Silber, J. J.; Falcone, R. D. Catanionic reverse micelles as an optimal microenvironment to alter the water electron donor capacity in a SN2 reaction. *Journal of Organic Chemistry* **2019**, *84*, 1185−1191.
(69) Fuglestad, B.; Gupta, K.; Wand, A. J.; Sharp, K. A. Characterization of cetyltrimethylammonium bromide/hexanol reverse micelles by experimentally benchmarked molecular dynamics simulations. *Langmuir* **2016**, *32*, 1674−1684.
(70) Fayer, M. D. Dynamics of water interacting with interfaces, molecules, and ions. *Accounts of chemical research* **2012**, *45*, 3−14.
(71) Schulz, P. DSC analysis of the state of water in surfactant-based microstructures. *J. Therm. Anal. Calorim.* **1998**, *51*, 135−149.
(72) El Seoud, O. A.; Blaskó, A.; Bunton, C. A. Proton NMR studies on the structure of water at interfaces of aqueous micelles. Part 4: Effects of cationic and zwitterionic headgroups. *Berichte der Bunsengesellschaft f ü r physikalische Chemie* **1995**, *99*, 1214−1220.
(73) Nnyigide, O. S.; Lee, S.-G.; Hyun, K. In silico characterization of the binding modes of surfactants with bovine serum albumin. *Sci. Rep.* **2019**, *9*, 10643.
(74) Balasubramanian, S.; Pal, S.; Bagchi, B. Hydrogen-bond dynamics near a micellar surface: origin of the universal slow relaxation at complex aqueous interfaces. *Physical review letters* **2002**, *89*, No. 115505.
(75) Carlstroem, G.; Halle, B. Water dynamics in microemulsion droplets. A nuclear spin relaxation study. *Langmuir* **1988**, *4*, 1346−1352.
(76) Ekwall, P.; Mandell, L.; Solyom, P. The solution phase with reversed micelles in the cetyl trimethylammonium bromide-hexanol-water system. *J. Colloid Interface Sci.* **1971**, *35*, 266−272.
(77) Senapati, S.; Berkowitz, M. L. Water structure and dynamics in phosphate fluorosurfactant based reverse micelle: A computer simulation study. *J. Chem. Phys.* **2003**, *118*, 1937.
(78) Tokmakoff, A. Shining Light on the Rapidly Evolving Structure of Water. *Science* **2007**, *317*, 54−55.
(79) Chowdhary, J.; Ladanyi, B. M. Molecular Simulation Study of Water Mobility in Aerosol-OT Reverse Micelles. *J. Phys. Chem. A* **2011**, *115*, 6306−6316.
(80) Ghosh, A.; Ostrander, J. S.; Zanni, M. T. Watching Proteins Wiggle: Mapping Structures with Two-Dimensional Infrared Spectroscopy. *Chem. Rev.* **2017**, *117*, 10726−10759.
(81) Baryiames, C. P.; Teel, M.; Baiz, C. R. Interfacial H-Bond Dynamics in Reverse Micelles: The Role of Surfactant Heterogeneity. *Langmuir* **2019**, *35*, 11463−11470.
(82) Marti, J.; Nagy, G.; Guardia, E.; Gordillo, M. C. Molecular Dynamics Simulation of Liquid Water Confined inside Graphite Channels: Dielectric and Dynamical Properties. *J. Phys. Chem. B* **2006**, *110*, 23987−23994.
(83) Chakraborty, S.; Sinha, S. K.; Bandyopadhyay, S. Low-Frequency Vibrational Spectrum of Water in the Hydration Layer of a Protein: A Molecular Dynamics Simulation Study. *J. Phys. Chem. B* **2007**, *111*, 13626−13631.
(84) Sechler, T. D.; Delsole, E. M.; Deak, J. C. Measuring properties of interfacial and bulk water regions in a reverse micelle with IR

https://doi.org/10.1021/acs.jpcb.4c04773
J. Phys. Chem. B XXXX, XXX, XXX−XXX

spectroscopy: A volumetric analysis of the inhomogeneously broadened OH band. *J. Colloid Interface Sci.* **2010**, *346*, 391−397.
(85) Ikehata, A.; Nakamura, K.; Ozaki, Y. Extended molar absorption analysis of confined states of water in reverse micelles using near-infrared spectroscopy. *Chem. Phys. Lett.* **2022**, *806*, No. 140055.
(86) Martínez, L.; Andrade, R.; Birgin, E. G.; Martínez, J. M. PACKMOL: A package for building initial configurations for molecular dynamics simulations. *Journal of computational chemistry* **2009**, *30*, 2157−2164.
(87) Ladanyi, B. M. Computer simulation studies of counterion effects on the properties of surfactant systems. *Current opinion in colloid & interface science* **2013**, *18*, 15−25.
(88) Lang, J.; Mascolo, G.; Zana, R.; Luisi, P. L. Structure and dynamics of cetyltrimethylammonium bromide water-in-oil microemulsions. *J. Phys. Chem.* **1990**, *94*, 3069−3074.
(89) Gardner, A.; Vasquez, V.; Clifton, A.; Graeve, O. Molecular dynamics analysis of the AOT/water/isooctane system: Effect of simulation time, initial configuration, and model salts. *Fluid Phase Equilib.* **2007**, *262*, 264−270.
(90) Oostenbrink, C.; Villa, A.; Mark, A. E.; Van Gunsteren, W. F. A biomolecular force field based on the free enthalpy of hydration and solvation: the GROMOS force-field parameter sets 53A5 and 53A6. *Journal of computational chemistry* **2004**, *25*, 1656−1676.
(91) Liu, B.; Hoopes, M. I.; Karttunen, M. Molecular Dynamics Simulations of DPPC/CTAB Monolayers at the Air/Water Interface. *J. Phys. Chem. B* **2014**, *118*, 11723−11737.
(92) Dietz, W.; Heinzinger, K. Structure of liquid chloroform. A comparison between computer simulation and neutron scattering results. *Berichte der Bunsengesellschaft f ü r physikalische. Chemie* **1984**, *88*, 543−546.
(93) Tironi, I. G.; Van Gunsteren, W. F. A molecular dynamics simulation study of chloroform. *Mol. Phys.* **1994**, *83*, 381−403.
(94) Berendsen, H. J.; Grigera, J. R.; Straatsma, T. P. The missing term in effective pair potentials. *J. Phys. Chem.* **1987**, *91*, 6269−6271.
(95) Kumar, H.; Dasgupta, C.; Maiti, P. K. Structure, dynamics and thermodynamics of single-file water under confinement: Effects of polarizability of water molecules. *RSC Adv.* **2015**, *5*, 1893−1901.
(96) Van Der Spoel, D.; Lindahl, E.; Hess, B.; Groenhof, G.; Mark, A. E.; Berendsen, H. J. GROMACS: fast, flexible, and free. *Journal of computational chemistry* **2005**, *26*, 1701−1718.
(97) Abraham, M. J.; Murtola, T.; Schulz, R.; Páll, S.; Smith, J. C.; Hess, B.; Lindahl, E. GROMACS: High performance molecular simulations through multi-level parallelism from laptops to supercomputers. *SoftwareX* **2015**, *1*, 19−25.
(98) Hess, B.; Bakker, H.; Berendsen, H. J. C.; Fraaije, J. G. E. M. LINCS: A linear constraint solver for molecular simulations. *J. Comput. Chem.* **1997**, *18*, 1463−1472.
(99) Miyamoto, S.; Kollman, P. A. Settle: An analytical version of the SHAKE and RATTLE algorithm for rigid water models. *J. Comput. Chem.* **1992**, *13*, 952−962.
(100) Essmann, U.; Perera, L.; Berkowitz, M. L.; Darden, T.; Lee, H.; Pedersen, L. G. A smooth particle mesh Ewald method. *J. Chem. Phys.* **1995**, *103*, 8577−8593.
(101) Darden, T.; York, D.; Pedersen, L. Particle mesh Ewald: An N log (N) method for Ewald sums in large systems. *J. Chem. Phys.* **1993**, *98*, 10089−10092.
(102) Bussi, G.; Donadio, D.; Parrinello, M. Canonical sampling through velocity rescaling. *J. Chem. Phys.* **2007**, *126*, No. 014101.
(103) Bussi, G.; Zykova-Timan, T.; Parrinello, M. Isothermal-isobaric molecular dynamics using stochastic velocity rescaling. *J. Chem. Phys.* **2009**, *130*, No. 074101.
(104) Parrinello, M.; Rahman, A. Polymorphic transitions in single crystals: A new molecular dynamics method. *J. Appl. Phys.* **1981**, *52*, 7182−7190.
(105) Nosé, S.; Klein, M. Constant pressure molecular dynamics for molecular systems. *Mol. Phys.* **1983**, *50*, 1055−1076.
(106) Pluhařová, E.; Stirnemann, G.; Laage, D. On water reorientation dynamics in cation hydration shells. *J. Mol. Liq.* **2022**, *363*, No. 119886.
(107) Bandyopadhyay, D.; Mohan, S.; Ghosh, S. K.; Choudhury, N. Molecular dynamics simulation of aqueous urea solution: is urea a structure breaker? *J. Phys. Chem. B* **2014**, *118*, 11757−11768.
(108) Ayappa, K. G.; et al. Enhancing the Dynamics of Water Confined between Graphene Oxide Surfaces with Janus Interfaces: A Molecular Dynamics Study. *journal of physical chemistry. B* **2019**, *123*, 2978−2993.
(109) Laage, D.; Stirnemann, G.; Sterpone, F.; Rey, R.; Hynes, J. T. Reorientation and allied dynamics in water and aqueous solutions. *Annu. Rev. Phys. Chem.* **2011**, *62*, 395−416.
(110) Lin, S.; Tang, P.-H.; Wu, T.-M. Local structural effects on orientational relaxation of OH-bond in liquid water over short to intermediate timescales. *J. Chem. Phys.* **2014**, *141*, 214505.
(111) Shafiei, M.; von Domaros, M.; Bratko, D.; Luzar, A. Anisotropic structure and dynamics of water under static electric fields. *J. Chem. Phys.* **2019**, *150*, No. 074505.
(112) Soper, A.; Benmore, C. Quantum differences between heavy and light water. *Physical review letters* **2008**, *101*, No. 065502.
(113) Chau, P.-L.; Hardwick, A. J. A new order parameter for tetrahedral configurations. *Mol. Phys.* **1998**, *93*, 511−518.
(114) Luzar, A.; Chandler, D. Effect of Environment on Hydrogen Bond Dynamics in Liquid Water. *Phys. Rev. Lett.* **1996**, *76*, 928.
(115) Djikaev, Y.; Ruckenstein, E. Dependence of the number of hydrogen bonds per water molecule on its distance to a hydrophobic surface and a thereupon-based model for hydrophobic attraction. *J. Chem. Phys.* **2010**, *133*, 194105.
(116) Rana, M.; Chandra, A. Filled and empty states of carbon nanotubes in water: Dependence on nanotube diameter, wall thickness and dispersion interactions. *Journal of chemical sciences* **2007**, *119*, 367−376.
(117) Stillinger, F. H.; Rahman, A. Improved simulation of liquid water by molecular dynamics. *J. Chem. Phys.* **1974**, *60*, 1545−1557.
(118) Rapaport, D. C. Hydrogen bonds in water. *Mol. Phys.* **1983**, *50*, 1151−1162.
(119) Chandra, A. Dynamical Behavior of Anion-Water and Water-Water Hydrogen Bonds in Aqueous Electrolyte Solutions: A Molecular Dynamics Study. *J. Phys. Chem. B* **2003**, *107*, 3899−3906.
(120) Balucani, U.; Brodholt, J.; Vallauri, R. Analysis of the velocity autocorrelation function of water. *J. Phys.: Condens. Matter* **1996**, *8*, 6139.
(121) Farimani, A.; Aluru, N.; Tajkhorshid, E. Thermodynamic insight into spontaneous hydration and rapid water permeation in aquaporins. *Appl. Phys. Lett.* **2014**, *105*, No. 083702.
(122) Walrafen, G. E.; Chu, Y. C.; Piermarini, G. J. Low-Frequency Raman Scattering from Water at High Pressures and High Temperatures. *J. Phys. Chem.* **1996**, *100*, 10363−10372.
(123) Brubach, J. B.; Mermet, A.; Filabozzi, A.; Gerschel, A.; Roy, P. Signatures of the hydrogen bonding in the infrared bands of water. *J. Chem. Phys.* **2005**, *122*, 184509.
(124) Crupi, V.; Dianoux, A. J.; Majolino, D.; Migliardo, P.; Venuti, V. Dynamical response of liquid water in confined geometry by laser and neutron spectroscopies. *Phys. Chem. Chem. Phys.* **2002**, *4*, 2768−2773.
(125) Marti, J.; Padro, J. A.; Guardia, E. Molecular dynamics simulation of liquid water along the coexistence curve: Hydrogen bonds and vibrational spectra. *J. Chem. Phys.* **1996**, *105*, 639−649.

https://doi.org/10.1021/acs.jpcb.4c04773
J. Phys. Chem. B XXXX, XXX, XXX−XXX